H_3Se in the $Im\bar{3}m$ Phase: High-Pressure Superconductor with T_c Reaching 200 K at 64 GPa Mediated by Anharmonic Phonons

Yao Ma(马遥)[1], Mingqi Li(李明奇)[1], Wenjia Shi(史文佳)[1], Vei Wang(王伟)[1], Pugeng Hou(侯朴赓)[2*], and Mi Pang(庞蜜)[1*]

[1]*Department of Applied Physics, School of Sciences, Xi'an University of Technology, Xi'an 710054, China*
[2]*College of Science, Northeast Electric Power University, Changchun Road 169, Jilin 132012, China*

(Received 14 August 2024; accepted manuscript online 15 November 2024)

Hydrogen-based compounds have attracted significant attention in recent years due to the discovery of conventional superconductivity with high critical temperature under high pressure, rekindling hopes for finding room-temperature superconductors. In this study, we investigated the vibrational and superconducting properties of H_3Se in the $Im\bar{3}m$ phase under pressures of 50–200 GPa. Our approach combines the stochastic self-consistent harmonic approximation and first-principles calculations to account for the quantum and anharmonic effects of ions. According to the results, these effects significantly modify the crystal structure, increasing the inner pressure by approximately 8 GPa compared to situations in which they are ignored. The phonon spectra suggest that when these effects are considered, the crystal stabilizes at pressures as low as approximately 61 GPa, which is significantly lower than the previously predicted value of over 100 GPa. Our calculations also highlight the critical role of quantum and anharmonic effects on the electron–phonon coupling properties. Neglecting these factors can result in a significant overestimation of the superconducting critical temperature (T_c) by approximately 4 K (200 GPa) to 25 K (125 GPa). With anharmonic phonons, the T_c calculated from the Migdal–Eliashberg equations reaches 200 K ($\mu^\star = 0.1$, $\lambda = 4.1$) as the pressure decreases to 64 GPa, indicating that the crystal is a rare high-T_c superconductor at moderate pressures.

DOI: 10.1088/0256-307X/41/12/127402

Introduction. High critical temperature (T_c) superconductivity has remained one of the most attracting yet challenging issues in physics for decades. Among the advancements already achieved, the discovery of high T_c in hydrogen-based systems stabilized by high pressure has piqued considerable research interest in recent years.[1–10] The prosperity of this field originates far from the suspicion of Neil Ashcroft in several decades ago[11,12] that pressurized hydrogen or hydrogen-dominant alloys can exhibit superconductivity at high temperatures, and then is facilitated by the advancement of high-pressure experimental techniques using diamond anvil cells.[3,13] The achievement in H_3S with a T_c of 203 K at 155 GPa[14] and in LaH_{10} with T_c of 260 K at 180–200 GPa[15] sparked hope for room-temperature superconductors. Since then, the superconductivity of an increasing number of hydrogen-based compounds have been investigated both experimentally and theoretically.

In the prediction of superconducting hydrides, computational techniques based on density functional theory (DFT) combined with conventional superconducting theory[16–18] have been extensively applied and play a crucial role, such as in the famous cases of H_3S,[19] LaH_{10},[20] YH_6,[21] and many others.[22–37] A crucial part of the calculation of superconductivity is the treatment of ionic vibrations, from which the parameters describing the electron–phonon interaction can be obtained. The conventional methodology employs the density functional perturbation theory (DFPT),[38] where ions are treated as classical particles. The potential $V(\boldsymbol{R})$, known as the Born–Oppenheimer (BO) potential, is approximated by a Taylor expansion around the equilibrium positions of ions that minimize $V(\boldsymbol{R})$. Typically, this expansion includes up to second-order terms and is referred to as the harmonic approximation. Thus, it ignores the quantum fluctuations of ions and the anharmonic nature of the potential. Recent studies have emphasized the crucial impact of quantum and anharmonic effects on the structural, vibrational, and superconducting properties of many systems, especially hydrogen-based compounds.[20,27,39–48] For example, the experimentally obtained T_c in H_3S (approximately 200 K)[14] and in LaH_10 (approximately 250 K)[15,49] at high pressures can only be well explained by considering the quantum effect and anharmonicity.

Given the high T_c observed in H_3S, there is a natural interest in H_3Se, which is achieved by substituting S with its isoelectronic counterpart Se. However, to the best of our knowledge, reports on H_3Se are rare and controversial. Experimental synthesis and metallization of H_3Se under high pressure have not yet been achieved. Zhang *et al.*[50] reported the synthesis of H_3Se in the $Cccm$ phase at 23 GPa, which was later identified as $(H_2Se)_2H_2$.[51] Theoretical predictions by Heil *et al.*[52] for H_3Se in the $Im\bar{3}m$ phase suggested a T_c of 100 K at 190 GPa. Other

*Corresponding author. Email: pugeng_hou@neepu.edu.cn; pangmi@xaut.edu.cn

studies[53–55] have estimated T_c values ranging from 110 K to 118 K at 200 GPa. Ge *et al.*[56] reported a T_c of approximately 163 K, whereas Flores-Livas *et al.*[57] suggested approximately 130 K for the same compound at 200 GPa. In addition, various studies[53,57] have investigated the structural stability of H_3Se in the $Im\bar{3}m$ phase, indicating stability at pressures exceeding 100 and 166 GPa, respectively. However, none of these calculations explored the quantum and anharmonic effects of ions.

In this study, the vibrational and superconducting properties of H_3Se in the $Im\bar{3}m$ phase under pressures relatively lower than those used in previous studies, ranging from 50 to 200 GPa, were systematically investigated using first-principles calculations. The quantum and anharmonic effects of ionic vibrations were incorporated through the stochastic self-consistent harmonic approximation (SSCHA). In contrast to previous predictions,[53,57] our calculations demonstrate that the crystal remains dynamically stable above approximately 61 GPa due to quantum and anharmonic effects, which are essential below pressures previously thought necessary to achieve stability (109 GPa with harmonic calculations). Significant modifications were obtained in optical phonons, including softened bond-bending modes and hardened bond-stretching modes, impacting the electron–phonon coupling (EPC) properties and suppressing T_c significantly, by up to approximately 25 K at 125 GPa. With anharmonic phonons, the T_c calculated from the Migdal–Eliashberg equations, reached 200 K ($\mu^\star = 0.1$), and λ exceeded 4, as the pressure decreased to 64 GPa. This study offers valuable insights for experimentally confirming the superconducting properties of H_3Se.

Methods and Computational Details. Conventional first-principles methods calculate the vibrational properties of materials employing the harmonic approximation, which treats ions as classical particles. The potential $V(\boldsymbol{R})$ as a function of the ion configuration $\boldsymbol{R}$, known as the Born-Oppenheimer (BO) potential, is Taylor expanded up to second-order terms around the configuration in equilibrium $\boldsymbol{R}_0$ that minimizes $V(\boldsymbol{R})$. By diagonalizing the dynamical matrix

$$D^h_{ab} = \frac{1}{\sqrt{M_a M_b}} \frac{\partial^2 V(\boldsymbol{R})}{\partial R_a \partial R_b}\bigg|_{\boldsymbol{R}_0}, \tag{1}$$

one obtains frequencies of the vibrational quanta, i.e., the harmonic phonons. In this equation, a and b denote combined indices identifying the Cartesian coordinates of all ions; M_a and R_a denote the mass and position of atom a, respectively.

Despite the success of the harmonic approximation, neglecting the quantum and anharmonic effects of ions can lead to significant deviations in material properties related to ionic vibrations, as mentioned in Section 1. The recently proposed SSCHA is aimed at addressing this issue.[41,43,58–60] Without approximating the BO potential $V(\boldsymbol{R})$, the SSCHA rigorously incorporates the effects of quantum ionic fluctuations based on the variational minimization of the free energy, $F[\rho] = \min_{\tilde{\rho}} \mathcal{F}[\tilde{\rho}]$; with $\mathcal{F}[\tilde{\rho}] = E[\tilde{\rho}] - TS[\tilde{\rho}]$, retaining all anharmonic terms. $E[\tilde{\rho}] = \langle K + V(\boldsymbol{R})\rangle_{\tilde{\rho}}$ is the total energy with K being the kinetic energy operator. $\langle O\rangle_{\tilde{\rho}} = \mathrm{Tr}[O\tilde{\rho}]/\mathrm{Tr}[\tilde{\rho}]$ is the quantum average of the operator O taken at the trial density matrix $\tilde{\rho}$ of the system. T represents the temperature, and $S[\tilde{\rho}]$ represents entropy. For feasible implementation in practice, the trial density matrix $\tilde{\rho} = \tilde{\rho}_{\boldsymbol{\mathcal{R}},\boldsymbol{\Phi}}$ is constrained to guarantee the distribution probability of ionic positions to be a Gaussian type and centered at the centroid positions $\boldsymbol{\mathcal{R}}$ with a width $\boldsymbol{\Phi}$ decided by the quantum-thermal fluctuations around them. The SSCHA minimizes $\mathcal{F}[\tilde{\rho}_{\boldsymbol{\mathcal{R}},\boldsymbol{\Phi}}]$ as a function of $\boldsymbol{\mathcal{R}}$ and $\boldsymbol{\Phi}$. During each minimization step, an ensemble of random ionic configurations in a supercell is extracted from $\tilde{\rho}_{\boldsymbol{\mathcal{R}},\boldsymbol{\Phi}}$, and the total energy and forces of each configuration are calculated with the external *ab initio* code to obtain the free energy function and its derivatives with respect to $\boldsymbol{\mathcal{R}}$ and $\boldsymbol{\Phi}$. Using the derivatives, $\boldsymbol{\mathcal{R}}$, $\boldsymbol{\Phi}$, and $\tilde{\rho}_{\boldsymbol{\mathcal{R}},\boldsymbol{\Phi}}$ are updated to minimize the free energy based on preconditioned gradient descent. At the minimum, the obtained $\boldsymbol{\mathcal{R}}_{\mathrm{eq}}$ determines the averaged ionic positions, and the auxiliary force constants $\boldsymbol{\Phi}_{\mathrm{eq}}$ represent the fluctuations around these positions.

In the static limits,[41,61,62] phonon frequencies are determined from the eigenvalues of the mass-rescaled second-order derivatives of the free energy obtained at $\boldsymbol{\mathcal{R}}_{\mathrm{eq}}$,

$$D^F_{ab} = \frac{1}{\sqrt{M_a M_b}} \frac{\partial^2 F}{\partial R_a \partial R_b}\bigg|_{\boldsymbol{\mathcal{R}}_{\mathrm{eq}}} \tag{2}$$

known as the free-energy Hessian at $\boldsymbol{\mathcal{R}}_{\mathrm{eq}}$. This is the quantum anharmonic analog of the classical harmonic dynamical matrix $\boldsymbol{D}^h$ [Eq. (1)]. Note that the appearance of negative eigenvalues of $\boldsymbol{D}^F$ or $\boldsymbol{D}^h$ (imaginary phonon frequencies) indicates structural instability with or without the quantum and anharmonic effects. In addition to optimizing inner cell ionic positions, the SSCHA can relax the lattice parameters under a specified pressure, incorporating the quantum effects and anharmonicity. This is realized by replacing the BO potential with the free energy when computing the stress tensor.

For simplicity, calculations using the classical harmonic approximation are referred to as harmonic calculations, whereas those employing the SSCHA to include quantum and anharmonic effects are referred to as anharmonic calculations.

The Eliashberg spectral function

$$\alpha^2F(\omega) = \frac{1}{2\pi N(0) N_q} \sum_{\mu\boldsymbol{q}} \frac{\gamma_\mu(\boldsymbol{q})}{\omega_\mu(\boldsymbol{q})} \delta[\omega - \omega_\mu(\boldsymbol{q})] \tag{3}$$

is calculated at both the harmonic and anharmonic levels, where $\gamma_\mu(\boldsymbol{q})$ denotes the phonon linewidth due to the electron–phonon interaction at the wave vector $\boldsymbol{q}$ of mode μ; $N(0)$ denotes the density of states at the Fermi level; N_q denotes the number of phonon momentum points used for Brillouin zone (BZ) sampling; $\omega_\mu(\boldsymbol{q})$ represent phonon frequencies obtained by diagonalizing $\boldsymbol{D}^F$ or $\boldsymbol{D}^h$ during anharmonic or harmonic calculations. The EPC constant (λ) and average logarithmic frequency ($\omega_{\log}$) can be obtained directly from $\alpha^2F(\omega)$ as $\lambda = 2\int_0^\infty \mathrm{d}\omega(\alpha^2F(\omega)/\omega)$ and $\omega_{\log} = \exp((2/\lambda)\int_0^\infty \mathrm{d}\omega(\alpha^2F(\omega)\ln(\omega)/\omega))$, respectively.

The superconducting critical temperature (T_c) is derived from the Allen–Dynes-modified McMillan equation [17]

$$T_c = \frac{f_1 f_2 \omega_{\log}}{1.2} \exp\Big[-\frac{1.04(1+\lambda)}{\lambda - \mu^*(1+0.62\lambda)}\Big], \quad (4)$$

with μ^* being the Coulomb pseudopotential. Here, f_1 and f_2 are functions of λ, μ^*, and $\alpha^2F(\omega)$. For comparison, T_c is also calculated by solving the isotropic Migdal–Eliashberg equations [18] once $\alpha^2F(\omega)$ is obtained.

The *ab initio* calculations were performed using the QUANTUM ESPRESSO (QE) package, [63] employing ultrasoft pseudopotentials with the Perdew–Burke–Ernzerhof parametrization [64] of the exchange-correlation potential. The cutoff energies for the wave functions and density were set to 80 and 800 Ry, respectively. Integration over the BZ in the self-consistent calculations was performed using Methfessel–Paxton smearing with broadening of 0.01 Ry and a $24\times24\times24$ $\boldsymbol{k}$-point grid. Harmonic phonon calculations were performed on a $9\times9\times9$ $\boldsymbol{q}$-point grid using DFPT. [38] The SSCHA calculations were performed on a $3\times3\times3$ supercell containing 108 atoms, and the resulting anharmonic dynamical matrices were interpolated to the finer $9\times9\times9$ grid. The electron–phonon interaction was evaluated in both the harmonic and anharmonic cases with Gaussian smearing of 0.008 Ry.

Results and Discussion. Previous studies [53,57] have suggested that H_3Se can be stabilized in the high-symmetry $Im\bar{3}m$ phase under pressures greater than 100 GPa. In this study, we focus on this structure and apply a wider range of pressures to explore the impact of quantum ionic fluctuations on its structural and vibrational properties. As shown in the corner of Fig. 1, this structure exhibits body-centered symmetry, each Se atom has six H atoms as the nearest neighbors located at the six corners of a regular octahedron centered on the Se atom, and the situation is similar for each H atom. Through harmonic and anharmonic calculations, structural deformation under external pressure is investigated. The pressure dependence of the lattice parameter is shown in Fig. 1. The quantum and anharmonic effects significantly correct the stress between ions. For the same lattice parameter, the pressure obtained from the harmonic calculations (referred to as harmonic pressure) is approximately 8 GPa lower than that obtained from the SSCHA (referred to as the anharmonic pressure). In contrast, the slope of the pressure with respect to the lattice parameter is barely affected. This stress correction is a commonly observed feature among superhydrides, such as AlH_3 [40] and $AlMH_6$. [65] Our calculations are consistent with those reported in previous studies, as shown by the triangle in Fig. 1.

Figure 2 shows the phonon spectra and the corresponding projected phonon density of states (PDOS) and the Eliashberg function $\alpha^2F(\omega)$ of H_3Se in the $Im\bar{3}m$ phase across a wide pressure range of 75–200 GPa based on both the harmonic approximation and SSCHA.

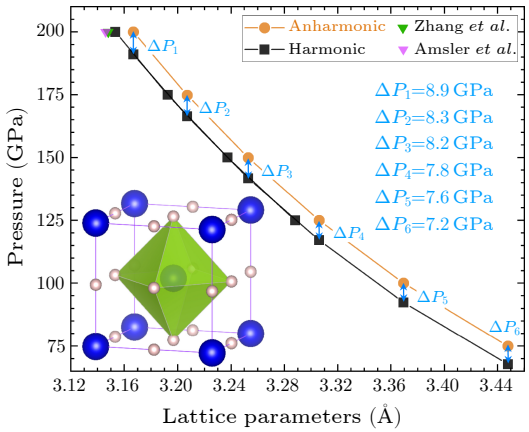

Fig. 1. Crystal structure and lattice parameter dependence on external pressure. The crystal structure of $Im\bar{3}m$ H_3Se is shown in the corner, where Se atoms are represented by blue spheres and H atoms by pink spheres. One of the polyhedra surrounding the central Se atom is depicted. The dependence of the lattice parameter on pressure is calculated at both the harmonic (black squares) and anharmonic (orange dots) levels. The results reported by Zhang *et al.* [53] and Amsler [54] are shown by colored triangles.

The anharmonic pressure (orange text) and the corresponding harmonic pressure (black text) of the same crystal structure are marked on each spectrum panel. Similar to the case in AlH_3, [40] under low pressures less than 109 GPa [see panels (a1) and (b1) of Fig. 2], the harmonic calculation yields negative (actually imaginary) phonon frequencies, most notably at the Γ point, indicating structural instability. This prediction is roughly consistent with that in Ref. [57]. However, the anharmonic phonon frequencies obtained from $\boldsymbol{D}^F$ remain positive in the 75–200 GPa range, highlighting the crucial role of quantum and anharmonic effects in stabilizing the $Im\bar{3}m$ phase of H_3Se under low pressures. To determine the minimum pressure required to stabilize the crystal in the anharmonic case, additional anharmonic calculations were performed in a low-pressure range of 50–64 GPa (see Fig. 3). The results reveal the emergence of imaginary anharmonic phonons under pressures of approximately 60 GPa. Interpolation analysis of the dependence of the lowest optical phonon frequency on pressure suggests that the minimum pressure required to stabilize the crystal is approximately 61 GPa.

Within the 100–200 GPa pressure range, the acoustic phonon branches are separated from the optical branches and are barely influenced by the quantum and anharmonic effects. This is because the acoustic modes predominantly involve contributions from heavy selenium atoms, as evidenced by the phonon partial density of states (PDOS) [Figs. 2(a2)–2(f2)]. In contrast, the optical phonons are significantly affected by quantum effects and anharmonicity in a manner that the six middle bond-bending branches are roughly softened, whereas the three high-energy bond-stretching branches are hardened, except the Γ point. Note that under low pressures, the bond-bending and bond-stretching branches are highly mixed. As shown

in Figs. 2(a2)–2(f2), hydrogen is the primary contributor to these optical modes. The anharmonic phonon linewidth due to the electron–phonon interaction is represented by red dots in Figs. 2(a1)–2(f1); the red dot size indicates strong coupling between bond-stretching phonons and electrons. Thus, these modes contribute significantly to T_c.

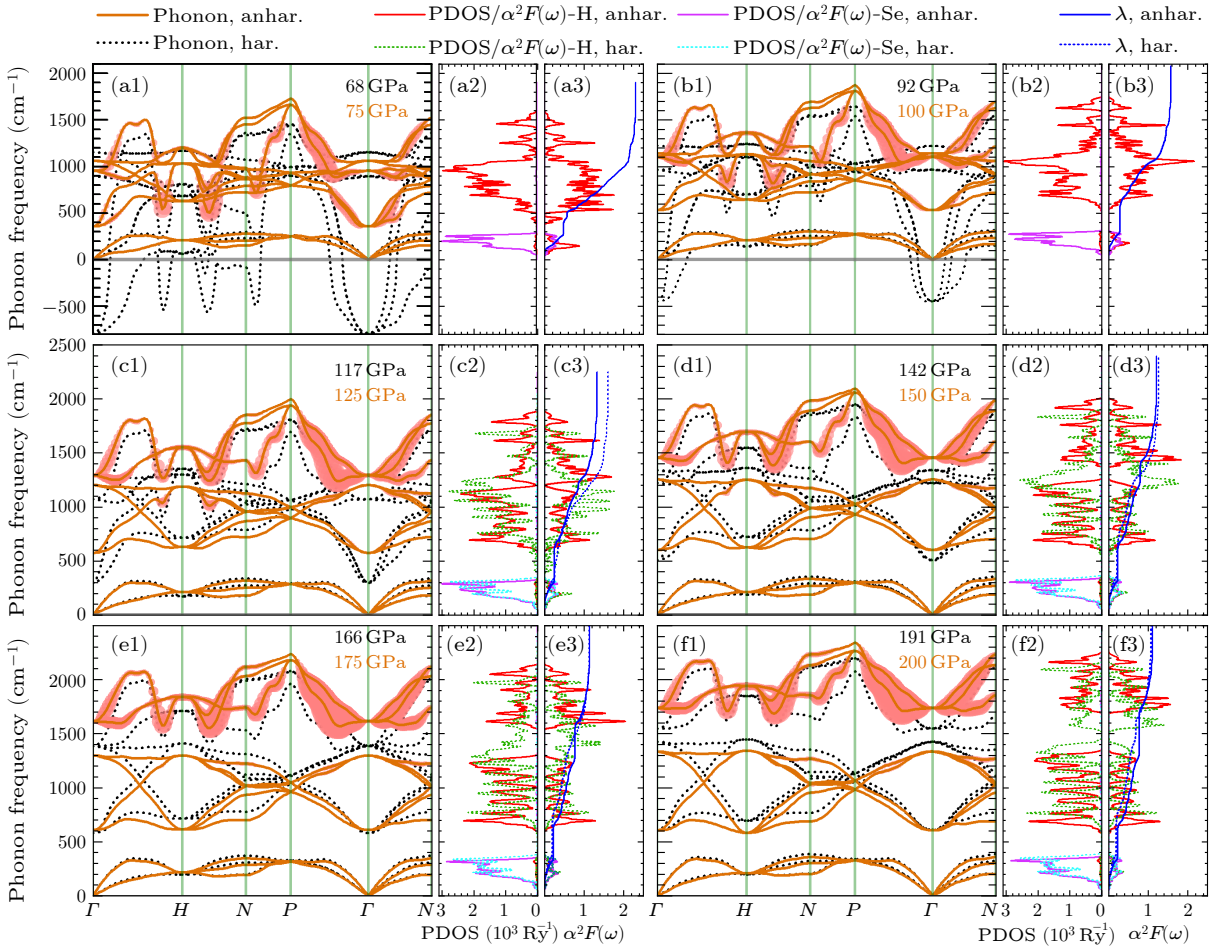

Fig. 2. (a1)–(f1) Comparison of harmonic (dotted lines) and anharmonic (solid lines) phonon spectra of $Im\bar{3}m$ H_3Se under pressures of 75–200 GPa. The corresponding harmonic pressures are also marked on each panel with black text. The anharmonic phonon linewidth of each mode due to the electron–phonon interaction is denoted by the size of the red dots in arbitrary units. Zero frequencies are indicated by the gray lines. (a2)–(f2) The PDOS and (a3)–(f3) the projected Eliashberg function $\alpha^2F(\omega)$ corresponding to the spectrum, where the solid and dotted lines denote the anharmonic and harmonic calculations, respectively, the red/green lines denote the contributions from H, and the magenta/cerulean lines denote the contributions from Se. The EPC constant λ is depicted by blue lines in (a3)–(f3).

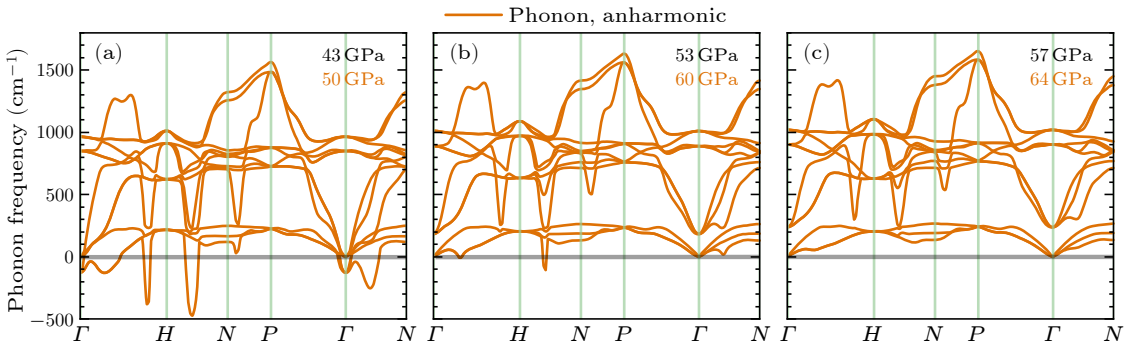

Fig. 3. Anharmonic phonon dispersions at (a) 50, (b) 60, and (c) 64 GPa. The harmonic pressures corresponding to the same crystal are denoted by black text in each panel.

The strong anharmonic modification of the optical phonons has a significant impact on the calculated T_c. Figure 4 show the T_c obtained from the Allen–Dynes-modified McMillan equation with the harmonic approximation and by combining the SSCHA with the EPC matrix elements, which are called harmonic T_c and anharmonic T_c respectively, for conciseness. The Coulomb pseudopotential parameter μ^* is selected as a typical value of 0.1 [Fig. 4(a)] and 0.13 [Fig. 4(b)]. We also solved the Migdal–Eliashberg equation [18] to obtain more accurate results. The Allen–Dynes equation underestimates T_c by 16–50 K compared with the Migdal–Eliashberg equation at pressures of 64–200 GPa for both harmonic and anharmonic calculations. In the strong EPC case at 75 GPa, the underestimation of T_c by the Allen–dynes equation can reach 30 K ($\mu^* = 0.1$)–34 K ($\mu^* = 0.13$), which is 16%–19% of T_c.

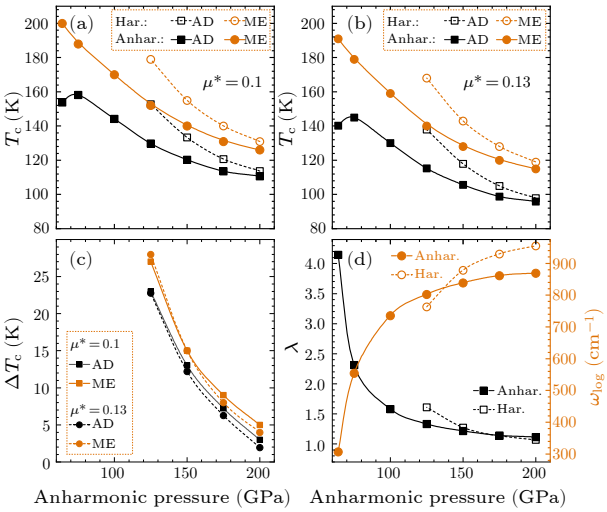

Fig. 4. Calculated T_c of $Im\bar{3}m$ phase of H_3Se as a function of anharmonic pressure. μ^* is selected as (a) 0.1 and (b) 0.13. T_c values calculated with the harmonic approximation (harmonic T_c) are denoted by hollow symbols, and those calculated by combining the SSCHA and the EPC matrix (anharmonic T_c) are denoted by solid symbols. Label 'AD' represents results obtained from the Allen–Dynes-modified McMillan equation, and 'ME' indicates results obtained from the Migdal–Eliashberg equation. (c) Amount by which harmonic T_c exceeds anharmonic T_c, denoted as ΔT_c. (d) EPC constant λ (black symbols) and average logarithmic frequency ω_{log} (orange symbols).

At 200 GPa, the T_c obtained from the Allen–Dynes equation with $\mu^* = 0.1$ in the harmonic calculation is 113.6 K, consistent with previous predictions. [53–55] For a given μ^*, T_c decreases monotonically with increasing pressure in both the harmonic and anharmonic calculations irrespective of whether the Allen–Dynes or Migdal–Eliashberg equation is used. The suppression of T_c by pressure primarily results from the overall hardening of the optical phonon modes imposed by compression. This can be understood from the Allen–Dynes equation (4), where T_c increases monotonically with the EPC constant λ within the typical parameter range. From the formula of λ as $\sum_{\mu\boldsymbol{q}} \gamma_\mu(\boldsymbol{q})/[\pi\hbar D(\epsilon_F)\omega_\mu^2(\boldsymbol{q})]$, which can be deduced from $\lambda = 2\int_0^\infty d\omega(\alpha^2F(\omega)/\omega)$ and Eq. (3), it can be concluded that λ, so as T_c decreases as the vibrations harden (phonon frequencies increase) and vice versa. λ and the average logarithmic frequency ω_{log} are presented in Fig. 4(d).

T_c is significantly overestimated in the harmonic approximation due to the neglect of the quantum and anharmonic effects. The overestimated amount of T_c, ΔT_c, i.e., harmonic T_c minus anharmonic T_c, is presented in Fig. 4(c). The overestimation of T_c reaches approximately 25 K at 125 GPa and decreases with increasing pressure to approximately 4 K at 200 GPa. For further exploration, the projected Eliashberg spectral function $\alpha^2F(\omega)$ and its integral $\lambda(\omega) = \int_0^\omega 2(\alpha^2F(\omega')/\omega')d\omega'$, for the harmonic and anharmonic cases are shown in Figs. 2(a3)–2(f3). The projected $\alpha^2F(\omega)$ onto H and Se can be obtained by calculating the partial contributions from different types of atoms to the phonon linewidth $\gamma_\mu(\boldsymbol{q})$ in Eq. (3). As shown in Figs. 2(a3)–2(f3), the contribution of the low-energy acoustic modes to λ is approximately 0.3 at 100 GPa and nearly 0.25 at pressures of 125–200 GPa, which is almost unaffected by the anharmonic effects. This is different from the case of AlH_3, [40] where the contribution of the acoustic modes is significantly suppressed by anharmonicity. The main contributors to $\alpha^2F(\omega)$ are optical phonons, which primarily originate from hydrogen atom vibrations.

As shown in Figs. 2(a3)–2(f3) and Fig. 4(d), λ is not notably suppressed by anharmonicity at high pressures of 150–200 GPa. λ, including anharmonicity, is even larger than that with harmonic calculations under 200 GPa [see blocks in Fig. 4(d)], different from the situations in AlH_3. [40] This can be interpreted as the result of a cancelation effect between the softening of bond-bending optical vibrations and the hardening of bond-stretching vibrations, which are influenced by anharmonicity. Suppression of T_c by anharmonicity under pressures of 150–200 GPa can be explained by the significant suppression of the Allen–Dynes average logarithmic phonon frequency ω_{log} by anharmonicity [see Fig. 4(d)]. ω_{log} is reduced from 930 to 861 cm^{-1} at 175 GPa and from 955 to 869 cm^{-1} at 200 GPa by the quantum and anharmonic effects, accounting for the decrease in T_c, even though λ is slightly increased when the anharmonic modification is performed.

Notably, at 64 GPa, T_c calculated from the Migdal–Eliashberg equations reaches 200 K ($\mu^\star = 0.1$), and λ exceeds 4, revealing that the $Im\bar{3}m$ H_3Se is a rare high-T_c superconducting hydride at moderate pressures. The large λ value may explain the deviation of the Allen–Dynes equation-calculated T_c from the pressure dependence of T_c at higher pressures [Figs. 4(a) and 4(b)], because the Allen–Dynes equation tends to yield inaccurate results in the case of strong EPC (large λ). [66]

Summary. In summary, we systematically investigated the vibration and superconducting properties of the $Im\bar{3}m$ phase of selenium hydride H_3Se using the SSCHA combined with DFT to incorporate quantum and anharmonic modifications. The results demonstrate that the crystal structure is significantly influenced by these modifications. The calculated pressure was approximately 8 GPa larger when considering quantum and anharmonic effects rather

than simply calculating with the traditional harmonic approximation for the same crystal structure with lattice parameters ranging from 3.17 to 3.45 Å. The phonon spectra were also significantly altered, as characterized by the overall softening of middle optical phonons and hardening of high-energy phonons. In particular, the phonon spectra imply that the structural instability predicted by harmonic calculations below 109 GPa is invalid when anharmonic modifications are considered, and the crystal remains stable at approximately 61 GPa. Modification of ionic vibrational properties exert a significant effect on the calculated superconducting critical temperature T_c such that the T_c obtained from the harmonic approximation is significantly suppressed by anharmonicity, such as from 153 K to 130 K at 125 GPa and from 121 K to 113 K at 175 GPa, obtained from the Allen–Dynes equation. Notably, at 64 GPa, where the crystal maintains dynamically stable facilitated by the quantum and anharmonic effects of ions, the T_c calculated from the Migdal–Eliashberg equations reaches 200 K, revealing that this crystal is a rare high-T_c superconducting hydride at moderate pressures. We analyzed the EPC properties and calculated parameters, such as the phonon linewidth and the Eliashberg spectral function. These data indicate that almost all corrections to T_c due to the quantum and anharmonic effects stem from their influence on hydrogen atom vibrations. This highlights the indispensable role of quantum and anharmonic effects in the estimation of the ionic vibration-related properties of hydrogen selenide, akin to many other hydrogen-based compounds. This study augments the dataset of the systematic properties of hydrogen-rich compounds, providing a foundation for further exploration into the essence of superconductivity.

Acknowledgements. This study was supported by the Natural Science Foundation Project (Grant No. 20230101280JC) of Jilin Provincial Department of Science and Technology.

References

[1] Gor'kov L P and Kresin V Z 2018 *Rev. Mod. Phys.* **90** 011001
[2] Sun W, Kuang X, Keen H D J, Lu C, and Hermann A 2020 *Phys. Rev. B* **102** 144524
[3] Flores-Livas J A, Boeri L, Sanna A, Profeta G, Arita R, and Eremets M 2020 *Phys. Rep.* **856** 1
[4] Kong P P, Minkov V S, Kuzovnikov M A, Drozdov A P, Besedin S P, Mozaffari S, Balicas L, Balakirev F F, Prakapenka V B, Chariton S *et al.* 2021 *Nat. Commun.* **12** 5075
[5] Chen B, Conway L J, Sun W, Kuang X, Lu C, and Hermann A 2021 *Phys. Rev. B* **103** 035131
[6] Zhang Z, Cui T, Hutcheon M J, Shipley A M, Song H, Du M, Kresin V Z, Duan D, Pickard C J, and Yao Y 2022 *Phys. Rev. Lett.* **128** 047001
[7] Minkov V S, Bud'ko S L, Balakirev F F, Prakapenka V B, Chariton S, Husband R J, Liermann H P, and Eremets M I 2022 *Nat. Commun.* **13** 3194
[8] Sun Y, Zhong X, Liu H, and Ma Y 2024 *Natl. Sci. Rev.* **11** nwad270
[9] Eremets M I 2024 *Natl. Sci. Rev.* **11** nwae047
[10] Cui W and Li Y 2019 *Chin. Phys. B* **28** 107104
[11] Ashcroft N W 1968 *Phys. Rev. Lett.* **21** 1748
[12] Ashcroft N W 2004 *Phys. Rev. Lett.* **92** 187002
[13] Boehler R and De Hantsetters K 2004 *High Pressure Research* **24** 391
[14] Drozdov A P, Eremets M I, Troyan I A, Ksenofontov V, and Shylin S I 2015 *Nature* **525** 73
[15] Somayazulu M, Ahart M, Mishra A K, Geballe Z M, Baldini M, Meng Y, Struzhkin V V, and Hemley R J 2019 *Phys. Rev. Lett.* **122** 027001
[16] Bardeen J, Cooper L N, and Schrieffer J R 1957 *Phys. Rev.* **108** 1175
[17] Allen P B and Dynes R C 1975 *Phys. Rev. B* **12** 905
[18] Allen P B and Mitrović B 1983 *Solid state physics* **37** 1
[19] Duan D, Huang X, Tian F, Li D, Yu H, Liu Y, Ma Y, Liu B, and Cui T 2015 *Phys. Rev. B* **91** 180502
[20] Errea I, Belli F, Monacelli L, Sanna A, Koretsune T, Tadano T, Bianco R, Calandra M, Arita R, Mauri F *et al.* 2020 *Nature* **578** 66
[21] Peng F, Sun Y, Pickard C J, Needs R J, Wu Q, and Ma Y 2017 *Phys. Rev. Lett.* **119** 107001
[22] Gao G Y, Oganov A R, Li P F, Li Z W, Wang H, Cui T, Ma Y M, Bergara A, Lyakhov A O, Iitaka T *et al.* 2010 *Proceedings of the National Academy of Sciences* **107** 1317
[23] Kim D Y, Scheicher R H, Pickard C J, Needs R J, and Ahuja R 2011 *Phys. Rev. Lett.* **107** 117002
[24] Liu H, Li Y, Gao G, Tse J S, and Naumov I I 2016 *The Journal of Physical Chemistry C* **120** 3458
[25] Li Y, Hao J, Liu H, Tse J S, Wang Y, and Ma Y 2015 *Scientific Reports* **5** 9948
[26] Zhong X, Wang H, Zhang J, Liu H, Zhang S, Song H F, Yang G, Zhang L, and Ma Y 2016 *Phys. Rev. Lett.* **116** 057002
[27] Bianco R, Errea I, Calandra M, and Mauri F 2018 *Phys. Rev. B* **97** 214101
[28] Liang X W, Zhao S T, Shao C C, Bergara A, Liu H, Wang L, Sun R, Zhang Y, Gao Y, Zhao Z *et al.* 2019 *Phys. Rev. B* **100** 184502
[29] Liang X, Bergara A, Wang L, Wen B, Zhao Z, Zhou X F, He J, Gao G, and Tian Y 2019 *Phys. Rev. B* **99** 100505
[30] Zhang P, Sun Y, Li X, Lv J, and Liu H 2020 *Phys. Rev. B* **102** 184103
[31] Jiang M J, Hai Y L, Tian H L, Ding H B, Feng Y J, Yang C L, Chen X J, and Zhong G H 2022 *Phys. Rev. B* **105** 104511
[32] Zhao W, Duan D, Du M, Yao X, Huo Z, Jiang Q, and Cui T 2022 *Phys. Rev. B* **106** 014521
[33] Du M, Li Z, Duan D, and Cui T 2023 *Phys. Rev. B* **108** 174507
[34] Yang K, Cui W, Hao J, Shi J, and Li Y 2023 *Phys. Rev. B* **107** 024501
[35] Shi L T, Si J G, Turnbull R, Liang A K, Liu P F, and Wang B T 2024 *Phys. Rev. B* **109** 054512
[36] Chen W, Ma T, Huo Z, Yu H, Cui T, and Duan D 2024 *Phys. Rev. B* **109** 224505
[37] Liu S Y, Huo P Y, Jiang W Z, Yang R Y, and Liu Y H 2024 *Phys. Rev. B* **109** 104514
[38] Baroni S, de Gironcoli S, Dal Corso A, and Giannozzi P 2001 *Rev. Mod. Phys.* **73** 515
[39] Borinaga M, Errea I, Calandra M, Mauri F, and Bergara A 2016 *Phys. Rev. B* **93** 174308
[40] Hou P, Belli F, Bianco R, and Errea I 2021 *Phys. Rev. B* **103** 134305
[41] Monacelli L, Bianco R, Cherubini M, Calandra M, Errea I, and Mauri F 2021 *Journal of Physics: Condensed Matter* **33** 363001
[42] Belli F 2022 *Characterization of hydrogen based superconductors from first principles* (PhD thesis)
[43] Bianco R, Errea I, Paulatto L, Calandra M, and Mauri F 2017 *Phys. Rev. B* **96** 014111
[44] Ribeiro G A S, Paulatto L, Bianco R, Errea I, Mauri F, and Calandra M 2018 *Phys. Rev. B* **97** 014306
[45] Belli F and Errea I 2022 *Phys. Rev. B* **106** 134509
[46] Setty C, Baggioli M, and Zaccone A 2020 *Phys. Rev. B* **102** 174506

[47] Setty C, Baggioli M, and Zaccone A 2021 *Phys. Rev. B* **103** 094519
[48] Setty C, Baggioli M, and Zaccone A 2024 *Journal of Physics: Condensed Matter* **36** 173002
[49] Drozdov A P, Kong P P, Minkov V S, Besedin S P, Kuzovnikov M A, Mozaffari S, Balicas L, Balakirev F F, Graf D E, Prakapenka V B *et al.* 2019 *Nature* **569** 528
[50] Zhang X, Xu W, Wang Y, Jiang S, Gorelli F A, Greenberg E, Prakapenka V B, and Goncharov A F 2018 *Phys. Rev. B* **97** 064107
[51] Pace E J, Binns J, Dalladay-Simpson P, Howie R T, and Alvarez M P 2018 *Phys. Rev. B* **98** 106101
[52] Heil C and Boeri L 2015 *Phys. Rev. B* **92** 060508
[53] Zhang S, Wang Y, Zhang J, Liu H, Zhong X, Song H F, Yang G, Zhang L, and Ma Y 2015 *Scientific Reports* **5** 15433
[54] Amsler M 2019 *Phys. Rev. B* **99** 060102
[55] Chang P H, Silayi S, Papaconstantopoulos D A, and Mehl M J 2020 *Journal of Physics and Chemistry of Solids* **139** 109315
[56] Ge Y, Zhang F, and Yao Y 2015 arXiv preprint arXiv:1507.08525
[57] Flores-Livas J A, Sanna A, and Gross E K U 2016 *Eur. Phys. J. B* **89** 63
[58] Errea I, Calandra M, and Mauri F 2013 *Phys. Rev. Lett.* **111** 177002
[59] Errea I, Calandra M, and Mauri F 2014 *Phys. Rev. B* **89** 064302
[60] Monacelli L, Errea I, Calandra M, and Mauri F 2018 *Phys. Rev. B* **98** 024106
[61] Monacelli L and Mauri F 2021 *Phys. Rev. B* **103** 104305
[62] Lihm J M and Park C H 2021 *Phys. Rev. Res.* **3** L032017
[63] Giannozzi P, Baroni S, Bonini N, Calandra M, Car R, Cavazzoni C, Ceresoli D, Chiarotti G L, Cococcioni M, Dabo I *et al.* 2009 *Journal of physics: Condensed matter* **21** 395502
[64] Perdew J P, Burke K, and Ernzerhof M 1996 *Phys. Rev. Lett.* **77** 3865
[65] Hou P, Ma Y, Pang M, Cai Y, Shen Y, Xie H, and Tian F 2024 *The Journal of Chemical Physics* **161** 024504
[66] Xie S R, Quan Y, Hire A C, Deng B, DeStefano J M, Salinas I, Shah U S, Fanfarillo L, Lim J, Kim J *et al.* 2022 *npj Comput. Mater.* **8** 14